BIOCHEMISTRY
including biophysical chemistry & molecular biology

Article

pubs.acs.org/biochemistry

The Fifth Transmembrane Segment of Cystic Fibrosis Transmembrane Conductance Regulator Contributes to Its Anion Permeation Pathway

Jingyao Zhang[†,‡] and Tzyh-Chang Hwang*[,†,‡,§]

[†]Department of Biological Engineering, University of Missouri—Columbia, 254 Agricultural Engineering, Columbia, Missouri 65211, United States

[‡]Dalton Cardiovascular Research Center, University of Missouri—Columbia, 134 Research Park, Columbia, Missouri 65211, United States

[§]Department of Medical Pharmacology and Physiology, University of Missouri—Columbia, Medical Sciences Building, Columbia, Missouri 65212, United States

Supporting Information

ABSTRACT: Previous studies have identified several transmembrane segments (TMs), including TM1, TM3, TM6, TM9, TM11, and TM12, as pore-lining segments in cystic fibrosis transmembrane conductance regulator (CFTR), but the role of TM5 in pore construction remains controversial. In this study, we employed substituted cysteine accessibility methodology (SCAM) to screen the entire TM5 defined by the original topology model and its cytoplasmic extension in a Cysless background. We found six positions (A299, R303, N306, S307, F310, and F311) where engineered cysteines react to intracellular 2-sulfonatoethyl methanethiosulfonate ($MTSES^-$). Quantification of the modification rate of engineered cysteines in the presence or absence of ATP suggests that these six residues are accessible in both the open and closed states. Whole-cell experiments with external $MTSES^-$ identified only two positive positions (L323 and A326), resulting in a segment containing 11 consecutive amino acids, where substituted cysteines respond to neither internal nor external $MTSES^-$, a unique feature not seen previously in CFTR's pore-lining segments. The observation that these positions are inaccessible to channel-permeant thiol-specific reagent $[Au(CN)_2]^-$ suggests that this segment of TM5 between F311 and L323 is concealed from the pore by other TMs and/or lipid bilayers. In addition, our data support the idea that the positively charged arginine at position 303 poses a pure electrostatic action in determining the single-channel current amplitude of CFTR and the effect of an open-channel blocker glibencalmide. Collectively, we conclude that the cytoplasmic portion of CFTR's TM5 lines the pore. Our functional data are remarkably consistent with predicted structural arrangements of TM5 in some homology models of CFTR.

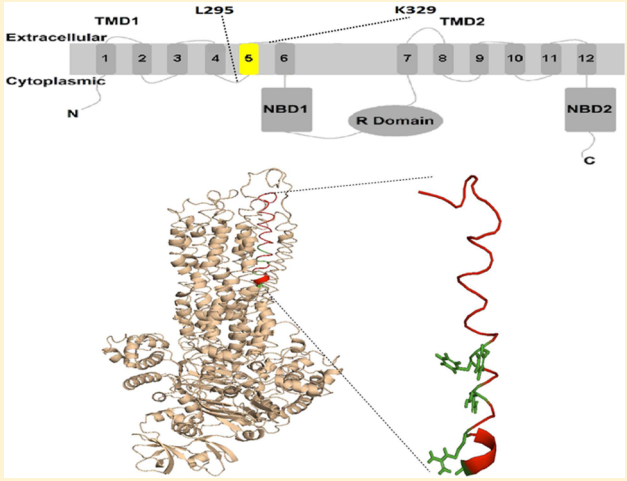

Members of the ATP binding cassette (ABC) protein superfamily enact the active movement of a broad range of cargos across the cell membrane against their electrochemical gradients through a translocation pathway embedded in their transmembrane domains (TMDs), whereas the conformational changes in the TMDs during a transport cycle are fueled by the free energy from ATP hydrolysis in the nucleotide binding domains (NBDs).[1,2] However, cystic fibrosis transmembrane conductance regulator (CFTR), a bona fide member of this superfamily, functions as a tightly regulated anion-selective ion channel, which is found mainly in the apical membrane of a host of epithelial cells.[3] Dysfunction of CFTR, resulting from loss-of-function mutations of the CFTR gene, causes the lethal recessively inherited disease cystic fibrosis.[4]

In addition to the basic architecture of the two TMD/NBD complexes seen in all ABC proteins, CFTR has a unique disordered regulatory domain (RD); its phosphorylation is a prerequisite for its activity.[5−8] It is now generally accepted that opening and closing (gating) of phosphorylated CFTR are controlled by the ATP-induced dimerization and hydrolysis-triggered partial separation, respectively, of CFTR's two NBDs, although how strictly these molecular motions are coupled

Received: April 20, 2015
Revised: May 18, 2015
Published: May 29, 2015

DOI: 10.1021/acs.biochem.5b00427
Biochemistry 2015, 54, 3839−3850

remains debatable.[9,10] Unlike NBDs that are evolutionarily conserved among ABC proteins, little sequence homology in TMDs makes it very difficult to predict their three-dimensional structure based on homology modeling that utilizes the crystal structures of ABC transporters[11−15] as templates. Nonetheless, several CFTR homology models have been developed.[16−20] It is perhaps not surprising that these structural models of CFTR all exhibit a 2-fold symmetry in their TMDs that is observed in the crystal structures of those ABC transporters. Recent studies using substituted cysteine accessibility methodology (SCAM) on CFTR's TMDs indeed support the idea that the aqueous pore is formed by some of the putative 12 transmembrane segments (TMs). These include TM1,[21] TM3,[22] TM6,[23,24] TM9,[16,25] TM11,[26] and TM12.[27,28] Furthermore, the reactivity patterns of the engineered cysteines in several TMs corroborate the predicted secondary structure of α-helix for TM1,[21] TM3,[22] TM6,[23] and TM12.[28] Also interestingly, state-dependent reactivity of the engineered cysteines in TM1, TM6, and TM12 endorses the "degraded transporter" hypothesis: CFTR evolves from a primordial ABC exporter with its cytoplasmic gate degenerated (ref 28, but cf. ref 29).

Although aforementioned studies suggest a 2-fold symmetry in CFTR's TMDs that is in agreement with the prediction based on the degraded transporter hypothesis, a recent paper reported experimental results contradicting this symmetry. First, by cysteine scanning nine positions in TM7 (F870−L878) of CFTR's TMD2, Wang et al.[30] concluded that this TM does not contribute to pore formation despite the fact that the corresponding TM (i.e., TM1) in TMD1 has been shown unequivocally to be part of the pore.[21,31] Second, by scanning six positions (F315−L320) in TM5 of TMD1 and seven residues (I1109−T1115) in its equivalent TM in TMD2 (i.e., TM11), they also concluded that the "central part" of TM11 but not of TM5 lines the pore.[30] The pore-lining role of TM11 is supported by previous work,[26] and those SCAM data on TM7 are also consistent with our observations using SCAM to probe a more extended region of TM7 (I860C to V880C) (Figure S1 of the Supporting Information). Moreover, it has been shown that several positively charged residues, including K95 in TM1,[32−34] R303 in TM5,[35,36] and R352 in TM6,[23,35,37−39] play critical roles in anion permeation by electrostatically attracting chloride ions to the internal entryway of CFTR's pore. Thus, it seems counterintuitive that both TM1 and TM6 line the pore but R303-containing TM5 does not.

In this study, we examined the role of TM5 in CFTR's pore construction with SCAM that covers the entire TM5 (S308−K329) and its cytoplasmic extension (L295−S307) in a Cysless background. By applying the negatively charged thiol-specific 2-sulfonatoethyl MTS ($MTSES^-$) from the cytoplasmic side of the membrane, we identified six positive hits, A299C, R303C, N306C, S307C, F310C, and F311C. The modification rates are somewhat higher in the absence of ATP than in the presence of ATP for cysteines placed at all these positions, implying that this segment of TM5 is slightly more accessible when the channel is in the closed state. Two $MTSES^-$-reactive positions, C323 and C326, were identified in the whole-cell configuration, when the reagent was applied from the extracellular side. The 11 positions between F311 and L323 were all negative to $MTSES^-$ applied from either side of the cell membrane. Cysteines introduced into these 11 positions were also insensitive to the channel-permeant, thiol-reactive $[Au(CN)_2]^-$ applied from intracellular side, suggesting that these 11 residues long enough to span at least three helical turns are not exposed to the aqueous pathway. We therefore conclude that TM5 does contribute to CFTR's pore in a way that distinguishes itself from other TMs. Our results will be discussed in the context of several homology models of CFTR.

EXPERIMENTAL PROCEDURES

Mutagenesis, Cell Culture, and Transient Expression. All experiments were performed in a Cysless CFTR construct reported previously.[23] Cysteine, one at a time, was then engineered into each position in originally defined TM5 (S308−K329) and its cytoplasmic extension (L295−S307) using the QuikChange XL kit (Agilent Technologies). All mutations were confirmed by DNA sequencing (DNA core; University of Missouri—Columbia).

Before transfection, the Chinese hamster ovary (CHO) cells were grown at 37 °C in Dulbecco's modified Eagle's medium containing 10% fetal bovine serum. Together with peGFP-C3 (Takara Bio Inc.) encoding green fluorescent protein, the cDNA constructs of CFTR were cotransfected into CHO cells, using PolyFect transfection reagent (QIAGEN) according to the manufacturer's instructions. The transfected cells were transferred onto sterile glass chips in 35 mm tissue culture dishes and incubated at 27 °C for 2−7 days before electrophysiological experiments were performed. The majority of our experiments require recordings of macroscopic CFTR currents. However, some mutations such as G314C display trafficking defects that prohibit an efficient membrane expression. We thus routinely incubated transfected cells at 27 °C for 2−7 days for CFTR channels to effectively move to the plasma membrane before electrophysiological experiments were performed. The majority of the CFTR constructs used in this study generated macroscopic CFTR chloride currents.

Electrophysiology. For experiments in excised inside-out patches, micropipettes made of borosilicate capillary glass were pulled with a two-stage vertical puller (Narishige) and then fire-polished with a homemade microforge to reach a pipet resistance of 2−5 MΩ when the pipettes were filled with a pipet solution containing 140 mM NMDG-Cl, 2 mM $MgCl_2$, 5 mM $CaCl_2$, and 10 mM HEPES, adjusted to pH 7.4 with NMDG. Glass chips with transfected cells grown on were placed into a chamber on the stage of an inverted microscope (Olympus) and continuously perfused with a bath solution containing 145 mM NaCl, 5 mM KCl, 2 mM $MgCl_2$, 1 mM $CaCl_2$, 5 mM glucose, 5 mM HEPES, and 20 mM sucrose, adjusted to pH 7.4 with NaOH. Immediately after patches with seal resistances of >40 GΩ had been excised, the perfusion solution was switched to a standard perfusate containing 150 mM NMDG-Cl, 10 mM EGTA, 10 mM HEPES, 8 mM Tris, and 2 mM $MgCl_2$, adjusted to pH 7.4 with NMDG. Experiments were conducted at room temperature (22−24 °C). Current signals at a −50 mV holding potential (unless specified otherwise) were acquired with a patch-clamp amplifier (EPC9, HEKA), filtered at 100 Hz digitized online at 500 Hz with Pulse software (version 8.53, HEKA), and captured onto a hard disk. Fast solution exchange was achieved with a commercial solution exchange system (SF-77B Perfusion Fast-Step, Warner Instruments).

Micropipettes used in whole-cell experiments were created as described above to yield a resistance of 1.5−2.5 MΩ when the micropipettes were filled with whole-cell pipet solution containing 10 mM EGTA, 10 mM HEPES, 20 mM TEACl, 10 mM MgATP, 2 mM $MgCl_2$, 85 mM aspartate, 16 mM pyruvate, and 5.8 mM glucose, with pH adjusted to 7.4 using

DOI: 10.1021/acs.biochem.5b00427
Biochemistry 2015, 54, 3839−3850

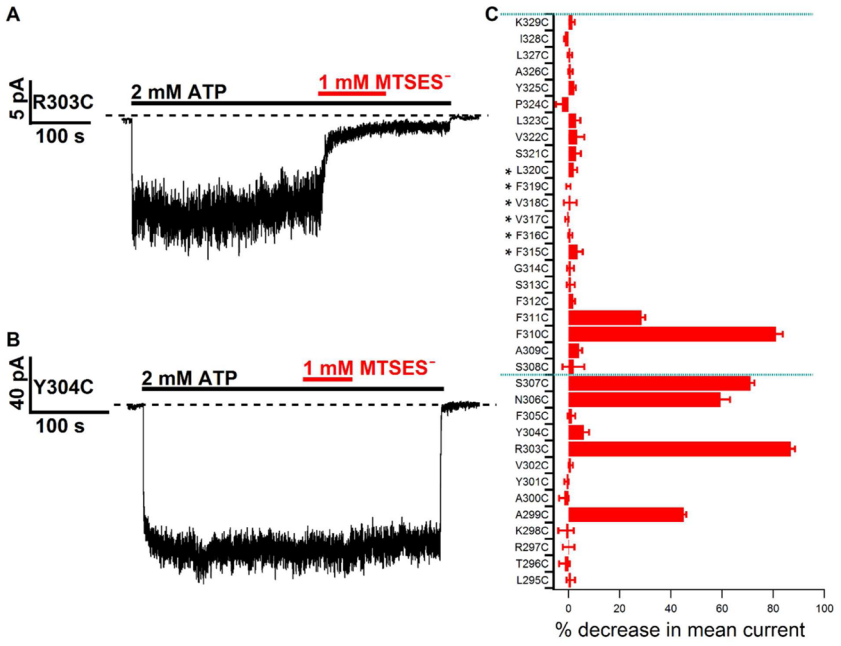

Figure 1. Cysteine scanning of TM5 in CFTR with intracellularly applied $MTSES^-$. (A) Representative current trace recorded at −50 mV in an inside-out membrane patch containing R303C-CFTR channels. The dashed line represents the baseline. Application of a saturating concentration of ATP elicited chloride currents (downward deflections). The ATP-induced CFTR current was reduced by intracellular $MTSES^-$ treatment. The decrease in current was not restored by the removal of $MTSES^-$, indicating that the decrease in current was likely due to a covalent modification of C303 by $MTSES^-$. (B) Representative recording of Y304C-CFTR channels using an experimental protocol similar to that described for panel A. The ATP-induced current was not altered upon intracellular $MTSES^-$ treatment, suggesting that the cysteine placed at position 304 is not accessible to intracellular $MTSES^-$. (C) Summary of the percent decrease in macroscopic mean currents after intracellular application of $MTSES^-$ for each cysteine-substituted channel (from cytoplasmic side L295C to extracellular side K329C). Asterisks mark the positions selected for SCAM studies by Wang et al.[30] The dotted lines mark the membrane boundaries depicted in the originally defined CFTR topology. n = 3–9. Data points in this and all subsequent figures are presented as means ± SEM.

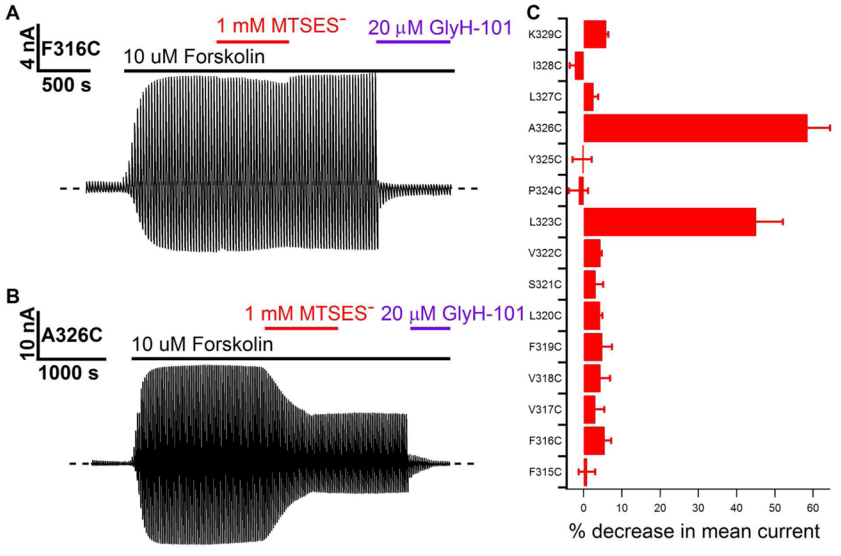

Figure 2. Cysteine scanning of CFTR TM5 with extracellularly applied $MTSES^-$ in the whole-cell configuration. (A) Representative recording of whole-cell currents from F316C-CFTR channels. The dashed line represents the zero current level. A voltage ramp ranging from −100 to 100 mV was applied every 5 s. After the currents were fully activated by forskolin, 1 mM $MTSES^-$ was applied extracellularly for several minutes until a steady state was reached. $MTSES^-$ was subsequently washed out. The final baseline conductance was obtained with 20 μM CFTR blocker GlyH-101 to abolish all residual CFTR currents. (B) Representative recording of whole-cell patch currents of A326C-CFTR channels using a protocol similar to that described for panel A. The CFTR current induced by forskolin decreased upon the application of extracellular $MTSES^-$. (C) Summary of the percentage decrease in macroscopic mean currents after the extracellular application of $MTSES^-$ for each cysteine-substituted channel (from cytoplasmic side F315C to extracellular side K329C). n = 3 or 4.

CsOH. During whole-cell experiments, cells were perfused with the same bath solution as the one used for inside-out recordings before patch excision. Experiments were conducted at room temperature (22–24 °C). Whole-cell currents were recorded

DOI: 10.1021/acs.biochem.5b00427
Biochemistry 2015, 54, 3839–3850

with a 200 ms voltage ramp of ±100 mV applied every 5 s. The signals were acquired with a patch-clamp amplifier (EPC9, HEKA), filtered at 1 kHz with an eight-pole Bessel filter (LPF-8, Warner Instruments), digitized online at 2 kHz with Pulse software (version 8.53, HEKA), and captured onto a hard disk.

Reagents and Cysteine Modification. MTS reagents [$MTSES^-$, $MTSET^+$, and $MTSEA^+$ (Toronto Research Chemicals Inc.)] were prepared as 100 mM stock solutions in ddH_2O and stored at −70 °C. A single aliquot of the stock solution was thawed immediately before use and diluted into the perfusion solution with or without 2 mM ATP (Sigma-Aldrich) to test the modification on cysteines in the presence of ATP (Figure 1) or in the absence of ATP (Figure 4), for experiments in inside-out patches. In the whole-cell configuration, the stock was thawed and diluted into the bath solution containing 10 μM forskolin (Figure 2). $K[Au(CN)_2]$ (Sigma-Aldrich) was prepared as 10 mM stock solutions and stored at 4 °C in a dry and sealed dark box to prevent degradation. During the experiment, $K[Au(CN)_2]$ was protected from light by wrapping the perfusion tubes with aluminum foil. PP_i and glibenclamide were purchased from Sigma-Aldrich Co. LLC. GlyH-101 was provided by the Chemical Compound Distribution Program sponsored by Cystic Fibrosis Foundation Therapeutics.

To measure the modification rate of $MTSES^-$ in the absence of ATP, we first applied 32 IU/mL PKA (Sigma-Aldrich) and 2 mM ATP to fully phosphorylate CFTR. Phosphorylated CFTR channels were subsequently opened with ATP for 3 s followed by a 13 s washout to determine the control peak mean current. The channels were then opened with ATP for 3 s followed by an 8 s washout; in the absence of ATP, $MTSES^-$ was applied for 3 s followed by a 2 s washout. This process was repeated 12 or 24 times depending on the time required for the modification to reach completion. The peak mean current amplitudes were plotted against cumulative application times of $MTSES^-$. This relationship was fitted with a single-exponential function to obtain the modification rate of $MTSES^-$ in the absence of ATP. To prevent the thiol group of engineered cysteine from undergoing spontaneous oxidation,[40,41] we routinely added 2.67 mM dithiothreitol (DTT) (Sigma-Aldrich) to the perfusion solution containing 32 IU/mL PKA and 2 mM ATP in the inside-out experiments, and 5 mM DTT to the bath solution containing forskolin in the whole-cell configuration.

Data Analysis. The single-channel current amplitude was estimated by Gaussian fitting of the all-point amplitude histogram with the multipeak fitting package in Igor Pro (WaveMetrics). For the modification of $MTSES^-$, the apparent second-order reaction rate constant was calculated as $1/(\tau[MTSES^-])$, where τ was measured by fitting the current decay phase upon the addition of $MTSES^-$ with a single-exponential function and $[MTSES^-]$ represents the working concentration of $MTSES^-$. All results are presented as means ± the standard error of the mean (SEM); n is the number of experiments. A Student's unpaired t test (two-tailed) was performed with Minitab16.2. $p < 0.05$ was considered significant. Figures of homology models were prepared with PyMOL (version 1.3, Schrödinger).

RESULTS

Reactivity of Substituted Cysteines in TM5 to Intracellular and Extracellular $MTSES^-$. To investigate the role of TM5 in CFTR's pore construction, we introduced cysteines, one at a time, into the originally defined TM5 (residues 308−329)[2] and its cytoplasmic extension (residues 295−307) in a Cysless background as described previously.[21,23,28] Each construct was then studied by assessing the reactivity of the substituted cysteines toward intracellularly applied, negatively charged $MTSES^-$. After inside-out patches containing cysteine-substituted channels were fully activated with 32 IU/mL PKA and 2 mM ATP, 1 mM $MTSES^-$ was applied in the presence of ATP for at least 1 min. We then switched the perfusion solution back to one with ATP alone to ensure that the current response is due to a covalent modification of the engineered cysteine by $MTSES^-$ and hence is not reversed by a simple removal of the reagent. In a representative recording of R303C-CFTR (Figure 1A), the comparison of the mean current before and after the $MTSES^-$ treatment shows an irreversible decrease in the mean current by ∼87%. In contrast, Figure 1B shows an experiment in which $MTSES^-$ does not affect the ATP-dependent current of Y304C-CFTR channels. Although we cannot rule out the possibility that the cysteine at position 304 was actually modified but without noticeable effects, the simplest explanation for this negative result is that the side chain of cysteine at this position is not exposed to the aqueous environment so as not to be modified by $MTSES^-$.

As seen in the summarized results (Figure 1C), six cysteine-substituted CFTR channels, including A299C, R303C, N306C, S307C, F310C, and F311C, responded to cytoplasmic application of $MTSES^-$. The apparent periodicity of these six reactive positions on TM5 suggests that the innermost part of TM5 and its cytoplasmic extension assume a secondary structure of α-helix as proposed previously.[42] Similar inference of an α-helical structure was made for other TMs (e.g., TM1, TM3, TM6, and TM12). Consistent with our previous SCAM studies of TM1, TM6, and TM12,[21,23,28] there is a clear accessibility limit in TM5 (position 311), beyond which cytoplasmic application of $MTSES^-$ fails to modify the engineered cysteine.

We next employed whole-cell patch-clamp techniques and applied $MTSES^-$ from the extracellular side of the membrane to identify positions that are accessible from the external end of the channel. Although R303C-, N306C-, and F310C-CFTR can be readily modified by internal $MTSES^-$, external $MTSES^-$ failed to alter whole-cell currents from any of these three constructs (data not shown). Surprisingly, after testing 15 cysteine-substituted constructs (positions 315−329), we identified only two positive hits (residues 323 and 326). Panels A and B of Figure 2 demonstrate representative whole-cell forskolin-activated CFTR currents in response to extracellular applications of $MTSES^-$: while 1 mM $MTSES^-$ has little effect on F316C-CFTR, it decreased A326C-CFTR currents by ∼50%. GlyH-101, a CFTR inhibitor,[43,44] was applied at the end of the experiments to ensure any currents that remained after the application of $MTSES^-$ are indeed from CFTR. Figure 2C summarizes these whole-cell experiments with external applications of $MTSES^-$.

Reactivity of Substituted Cysteines in TM5 to Intracellular $[Au(CN)_2]^-$. The results summarized in Figures 1C and 2C reveal a pattern very different from what we have reported for TM1, TM6, and TM12.[21,23,28] First, previously identified internal accessibility limits reside relatively close to the middle section of the characterized TMs (e.g., L102 in TM1, S341 in TM6, and M1140 in TM12), whereas F311 in TM5 is located close to the cytoplasmic end. Second, the narrow region of the pore, defined as the segment of TMs

DOI: 10.1021/acs.biochem.5b00427
Biochemistry 2015, 54, 3839−3850

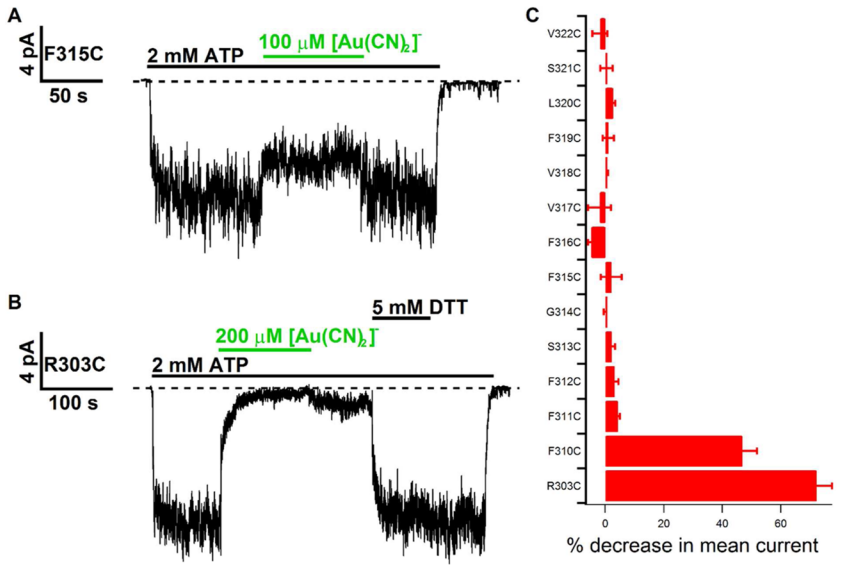

Figure 3. Effects of channel-permeant thiol-specific reagent $[Au(CN)_2]^-$ on cysteines introduced into TM5. (A) Continuous current trace recorded from an inside-out membrane patch containing F315C-CFTR channels. The dashed line represents the baseline current level. Application of a saturating concentration of ATP elicited chloride currents following activation of the channels by 32 IU/mL PKA and ATP (not shown). The ATP-induced current is decreased upon the addition of intracellular $[Au(CN)_2]^-$, but the current completely recovered after the removal of $[Au(CN)_2]^-$. (B) Representative current recording of R303C-CFTR channels under an experimental protocol similar to that described for panel A. The current decrease upon intracellular $[Au(CN)_2]^-$ treatment was not restored upon the removal of $[Au(CN)_2]^-$. However, the application of DTT restored all the current, indicating that the current decrease was due to covalent modification by $[Au(CN)_2]^-$. (C) Summary of the percentage decrease in macroscopic mean currents after intracellular application of $[Au(CN)_2]^-$ for each cysteine-substituted channel (from cytoplasmic side F311C to extracellular side V322C together with F310C and R303C as positive controls). n = 3−5.

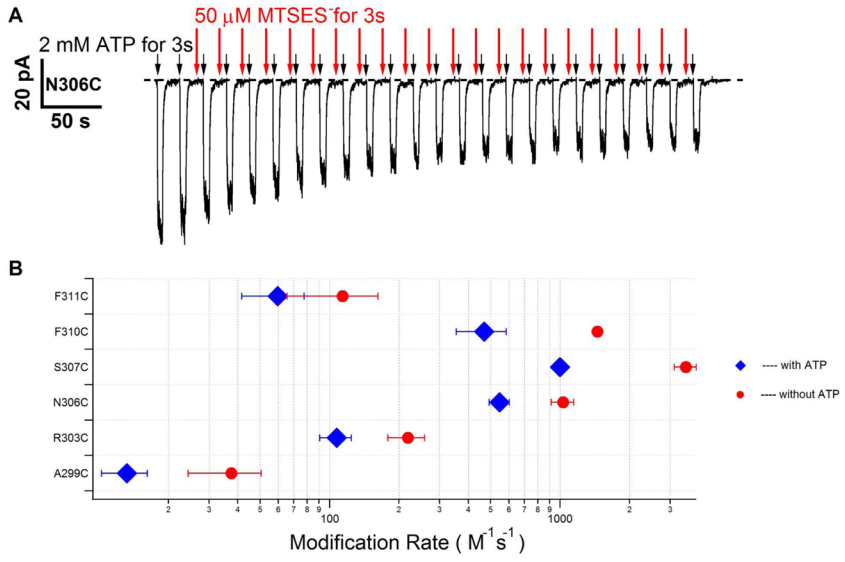

Figure 4. Quantitative assessments of modification rates by intracellular $MTSES^-$ in the absence and presence of ATP. (A) Representative result showing how the modification rate for intracellular $MTSES^-$ in the absence of ATP was estimated (see Experimental Procedures and Results for details). The dashed line represents the baseline current level. (B) Summary of $MTSES^-$ modification rates in the absence and presence of ATP at all six positive positions. n = 3−9.

between internal and external accessibility limits, spans only approximately two or three amino acids in TM1 and TM6 (i.e., L102−I106 in TM1 and S341−T338 in TM6), but cysteines placed at 11 positions between the internally accessible F311 and the externally accessible L323 do not react to either internal or external $MTSES^-$. One possible interpretation of these surprising observations is that this long stretch of TM5 is buried in the protein core and therefore does not line the pore. However, before this conclusion was reached, we considered another possibility: some of these 11 amino acids may line the pore but are not accessible because of the bulkiness of $MTSES^-$.

To exclude this possibility, we employed a channel-permeant thiol-specific reagent $[Au(CN)_2]^-$ to test if cysteines placed in any of these positions may react with internally applied $[Au(CN)_2]^-$. We reasoned that if some of these positions indeed line the narrow part of the anion permeation pathway, introducing a negatively charged adduct with $[Au(CN)_2]^-$

DOI: 10.1021/acs.biochem.5b00427
Biochemistry 2015, 54, 3839−3850

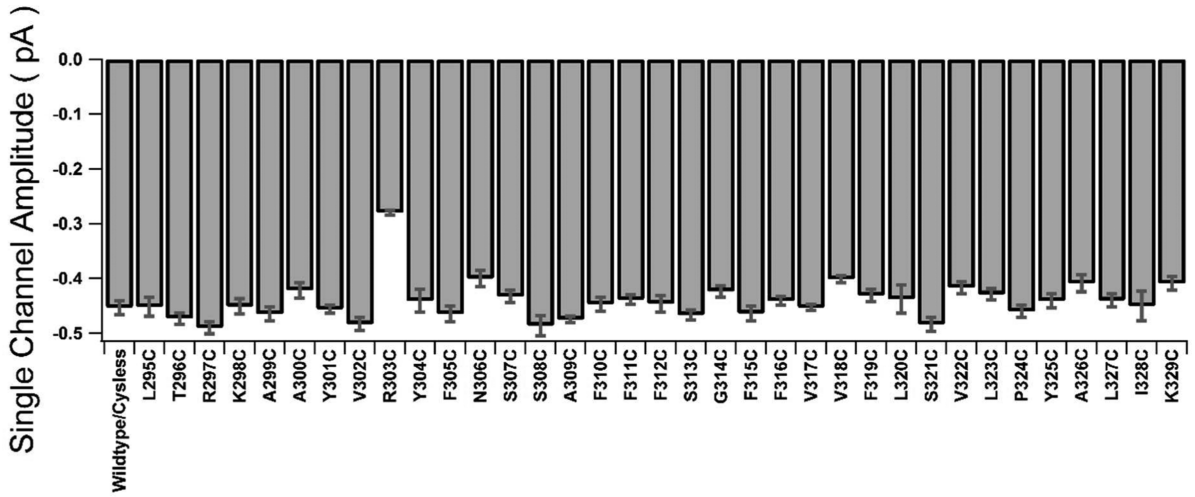

Figure 5. Summary of the single-channel current amplitude for WT/Cysless-CFTR and all cysteine-substituted channels. The transmembrane voltage was clamped at −50 mV. The data are shown as means ± SEM (n = 3−18). The only mutant that shows a dramatic difference in the single-channel current amplitude is R303C-CFTR.

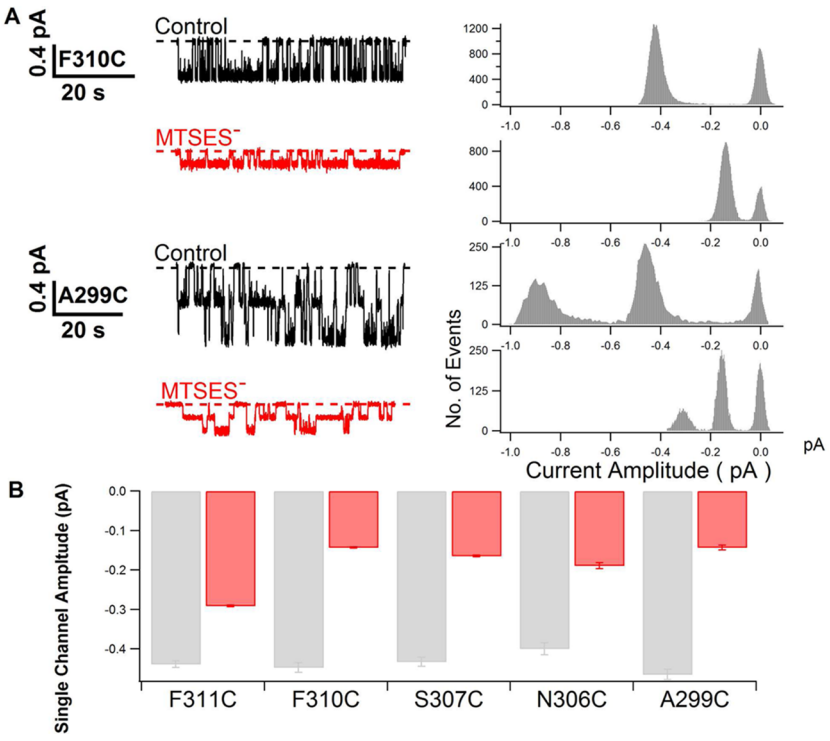

Figure 6. Modification by MTSES⁻ reduces the single-channel current amplitude of each reactive mutant. (A) Single-channel recordings of F310C- and A299C-CFTR showing a significant decrease in the single-channel current amplitude after the treatment with MTSES⁻. The dashed line represents the closed-state current level. All-point histograms of the corresponding current traces are presented to show the decrease in single-channel current amplitudes by MTSES⁻. (B) Summary of changes in the single-channel current amplitude before (gray) and after MTSES⁻ modification (red) at five reactive positions (n = 3−18) (the single-channel current amplitude of R303C-CFTR after MTSES⁻ modification is too small to be quantified accurately).

should decrease the current. Panels A and B of Figure 3 show representative results for two different constructs, F315C and R303C. In an inside-out patch (Figure 3A), application of 100 μM $[Au(CN)_2]^-$ after F315C-CFTR channels were opened by ATP caused a decrease in the current, but the current recovered completely once $[Au(CN)_2]^-$ was removed, indicating a reversible blockade of the channel by $[Au(CN)_2]^-$ as reported previously.[45] In contrast, a similar experimental protocol resulted in a significant decrease in the R303C-CFTR current and a simple washout of $[Au(CN)_2]^-$ did not restore the current amplitude (Figure 3B); however, a complete recovery was seen upon the addition of 5 mM dithiothreitol (DTT), a commonly used reducing reagent. Figure 3C summarizes all the results at these 11 positions and positions 303 and 310 as positive controls. We thus conclude that these 11 amino acids do not play a role in constructing the pore-lining segment of CFTR.

DOI: 10.1021/acs.biochem.5b00427
Biochemistry 2015, 54, 3839−3850

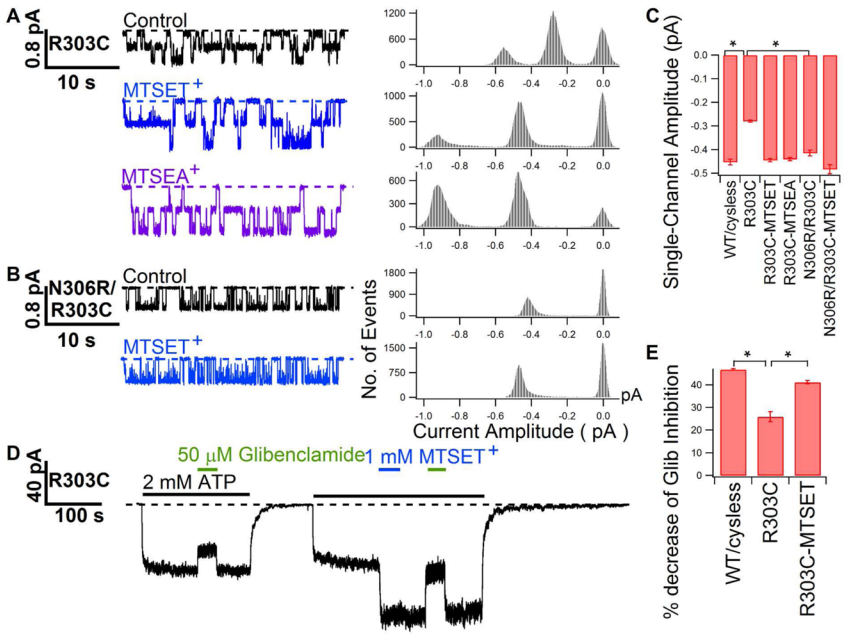

Figure 7. Effects of charge replacement at position 303. (A) Single-channel recordings demonstrating an increase in the single-channel current amplitude of R303C-CFTR after modification by $MTSET^+$ or $MTSEA^+$. The corresponding all-point histogram is presented to the right of each current trace. (B) Restoration of the single-channel current amplitude for R303C-CFTR by introducing a positively charged residue at position 306 (i.e., control of N306R/R303C-CFTR), and a further increase in the single-channel current amplitude by $MTSET^+$ modification. An all-point histogram for each single-channel trace is also presented. (C) Summary of the single-channel current amplitudes for R303C-CFTR and N306R/R303C-CFTR and those after modification by positively charged MTS reagents (n = 4−11). Asterisks mark statistically significant differences (p < 0.05). (D) Representative macroscopic current recording showing an increase in glibenclamide block after $MTSET^+$ modification on R303C-CFTR. The dashed line represents the closed-state current level. (E) Summary of glibenclamide block for WT/Cysless-CFTR, R303C-CFTR and $MTSET^+$-modified R303C-CFTR. Glib refers to glibenclamide. Asterisks mark statistically significant differences (p < 0.05). n = 4−7.

State-Dependent Modification of Engineered Cysteines in TM5 by $MTSES^-$. To further characterize those six positive positions identified by internal applications of $MTSES^-$, we compared the modification rates measured in the presence or absence of ATP (see Experimental Procedures for details). Figure 4A shows a representative experiment in which the modification rate in the absence of ATP was obtained for N306C-CFTR. After the channels were fully activated with PKA and ATP, ATP was applied for 3 s followed by an 8 s washout. As seen in Figure 4A, the first two applications of ATP elicited similar macroscopic current amplitudes. However, the currents induced by subsequent pulses of ATP show a gradual reduction as $MTSES^-$ was added in the washout solutions. Fitting the relationship between the relative current amplitude and cumulative washout time with a single-exponential function yields a time constant for calculating the modification rate of N306C in the absence of ATP.

Figure 4B summarizes our results. All six positions are accessible to internal applications of $MTSES^-$ regardless of whether the reagent is applied in the presence or absence of ATP. More interestingly, the modification rates in the absence of ATP are 2−4-fold higher than that in the presence of ATP in all six positions (Figure 4B), suggesting that these cysteines are accessible to cytoplasmic $MTSES^-$ in both open and closed states. Indeed, as seen in Figure S2 of the Supporting Information, N306C-CFTR can be modified when the channel is locked open by PP_i. These results also suggest that the inner vestibule of CFTR's pore, where these six residues reside, is more accessible in the closed state, a proposition consistent with previous work that shows a wider internal pore entrance in the closed state.[28]

Effects of Charge Replacement in the Inner Vestibule. So far, the results shown above with macroscopic recordings allow us to identify overall eight positions (of 35 scanned) at which engineered cysteines react with internal or external $MTSES^-$. Two possibilities lie behind the macroscopic mean current decrease caused by $MTSES^-$ modification. One is that the introduced adduct following $MTSES^-$ modification changes the single-channel current amplitude through either physically blocking the permeation pathway or electrostatically repulsing the passing chloride ions; the other possibility is that the $MTSES^-$ modification changes CFTR gating and hence reduces the open probability. Considering seriously this latter possibility is important in the current study for the following reasons. First, our previous reports have shown clear gating effects by chemical modification of cysteine-substituted CFTR.[21,23] Second, unlike what has been observed for TM1 and TM6, the single-channel current amplitude remains very constant in all cysteine-substituted CFTR mutants studied in this report, the only exception being R303C-CFTR (Figure 5).

We therefore examined the effect of $MTSES^-$ modification at the single-channel level. Two representative single-channel recordings and their all-point histograms (Figure 6A) show that before the application of $MTSES^-$, the single-channel current amplitudes of both F310C- and A299C-CFTR [−0.45 ± 0.01 pA (n = 10) and −0.49 ± 0.02 pA (n = 9), respectively] are very close to that of WT/Cysless-CFTR [−0.45 ± 0.01 pA (n = 5)], but the single-channel current amplitudes were dramatically decreased after the treatment of $MTSES^-$. Similar reductions in the single-channel current amplitude caused by

DOI: 10.1021/acs.biochem.5b00427
Biochemistry 2015, 54, 3839−3850

$MTSES^-$ treatment were also observed at positions N306C, S307C, and F311C. Figure 6B summarizes these microscopic studies on five cysteine-substituted constructs. The percent decrease in the single-channel current amplitude is close to the percent decrease in the macroscopic mean current, suggesting that even if any possible gating effect of modification is taken into consideration, most of the reduced macroscopic mean current is due to a decrease in the single-channel current amplitude (Figure S3 of the Supporting Information).

For R303C-CFTR, the only mutant with a reduced single-channel current amplitude [-0.28 ± 0.01 pA (Figure 7A,C)] because of the substitution of a positively charged arginine with a neural cysteine, the modification of negatively charged $MTSES^-$ further decreases the single-channel current amplitude to an unresolvable level (trace not presented). However, positively charged $MTSET^+$ or $MTSEA^+$ increases the single-channel current amplitude of R303C-CFTR to a level virtually identical to that of Cysless channels (Figure 7A,C). Thus, at position 303, a previously proposed pure electrostatic effect on chloride conductance seems at work.[35,36] Furthermore, in the R303C-CFTR background, when we replaced N306, a position approximately one helical turn external to R303, with an arginine, double mutant N306R/R303C-CFTR shows a single-channel current amplitude of -0.41 ± 0.01 pA ($n = 4$) higher than that of R303C-CFTR (Figure 7A–C), suggesting that moving the positive charge to a presumably neighboring residue can markedly restore the permeation property of the pore. The single-channel current amplitude of N306R/R303C-CFTR was further enhanced by the application of positively charged $MTSET^+$, supporting the idea that positively charged side chains at this region likely exert a favorable electrostatic attraction for permeating anions. The effect of charge replacement on the single-channel current amplitude of R303C-CFTR is summarized in Figure 7C.

The observation that CFTR's internal vestibule can accommodate multiple positively charged side chains (Figure 7, and also see ref 34) suggests that this part of the pore is fairly wide. This idea of a large internal vestibule in CFTR's anion permeation pathway is also supported by the observations that CFTR's pore can be blocked from the cytoplasmic side of the membrane by the large glibenclamide molecule (MW of 494).[46−50] Several previous studies have also established the critical role of an electropositive internal vestibule of CFTR in attracting anionic blockers such as glibenclamide.[23,28,50−52] This role of positive electropotential in promoting blockade of the pore by the glibenclamide is again demonstrated by our findings that the R303C mutation significantly reduces blockade of the pore by glibenclamide (Figure 7D), and this reduced block can be restored nearly to the full extent by $MTSET^+$ modification on R303C (Figure 7D,E). Collectively, these results of charge replacement experiments also support the notion that this part of TM5 does contribute to the ion permeation pathway.

DISCUSSION

The identification of pore-lining residues and the elucidation of relative motions of each TM during gating transitions are critical in shaping our understanding of the structural and functional properties of the CFTR chloride channel. In this study, we focused our efforts on characterizing CFTR's TM5 (S308–K329) and its cytoplasmic extension (L295–S307) with SCAM. Our investigations identified six positions, i.e., A299, R303, N306, S307, F310, and F311, where the engineered cysteine could be modified by intracellularly applied thiol-specific reagent $MTSES^-$. After $MTSES^-$ modification, the single-channel current amplitude is dramatically reduced as expected for an anion channel pore following the placement of a negatively charged adduct. Furthermore, the apparent periodicity of these six positions suggests that this cytoplasmic portion of TM5 assumes an α-helical secondary structure, an observation similar to our previous reports for TM1, TM6, and TM12.[21,23,28] Because cysteines introduced at all these positions can be modified both in the presence and in the absence of ATP, we inferred that the side chains of these six residues are exposed to the aqueous pore in both open and closed states. By comparing the modification rates of $MTSES^-$, we found that all six positions exhibit a higher rate of modification in the absence of ATP than in the presence of ATP (Figure 4), suggesting that these residues are more readily accessible when the channel resides in the closed state. If we accept the idea that this segment of TM5 forms part of the internal vestibule of the CFTR pore, this result is not surprising as previous SCAM studies of TM6 and TM12 implicate a widening of CFTR's internal pore entrance when the gate closes.[23,28] Moreover, our data show that the single-channel current amplitude of N306C can be reduced by $MTSES^-$ during one locked-opening burst (Figure S2 of the Supporting Information), invalidating the extreme scenario in which this cysteine at position 306 can be modified in only the closed state.

Notwithstanding similarities between TM5 and other TMs mentioned above, this study reveals an unexpected difference: there exists a segment of 11 consecutive amino acids (F312–V322), enough to span three helical turns, where the engineered cysteine fails to respond to internal or external $MTSES^-$. We also found no evidence of any reactivity for the introduced cysteines at these 11 positions to small channel-permeant, thiol-reactive $[Au(CN)_2]^-$. This unique feature distinguishes TM5 from other extensively studied TMs, such as TM1,[21,34] TM6,[16,23] and TM12,[16,27,28,53] where the accessibility limits to $MTSES^-$ from both sides of membrane are separated only by approximately two or three amino acid residues that are thought to form the narrowest region in the CFTR pore.[16] Although we cannot completely rule out other possibilities, the simplest explanation for these results is that this segment of TM5 is not exposed to the pore (also see below). Thus, different TMs may assume different structural roles in crafting the pore of CFTR. In fact, the observation that TM1 in CFTR's TMD1, but not its corresponding TM in TMD2 (i.e., TM7), contributes to pore lining indicates a significant asymmetry between TMD1 and TMD2 in the construction of the pore[30] (Figure S1 of the Supporting Information).

Despite some earlier reports implicating TM5 as a pore-lining segment,[31,35,36,54,55] this TM has not been subjected to SCAM studies extensively until recently. Following cysteine scanning of six positions (F315–L320) in TM5, Wang et al.[30] concluded that this fraction of TM5 does not play a role in pore construction. By contrast, in the same report, positive positions, including I1112, T1115, and S1118, were identified in TM11 (equivalent to TM5 in TMD2), suggesting that TM11 does contribute to pore lining, a conclusion supported by an earlier report.[26] Of note, the regions in TM5 and TM11 chosen by Wang et al.[30] for their SCAM studies were all located close to the "center" of each TM according to the originally defined topology of CFTR's TMDs.[2] The fact that the six positions in

DOI: 10.1021/acs.biochem.5b00427
Biochemistry 2015, 54, 3839−3850

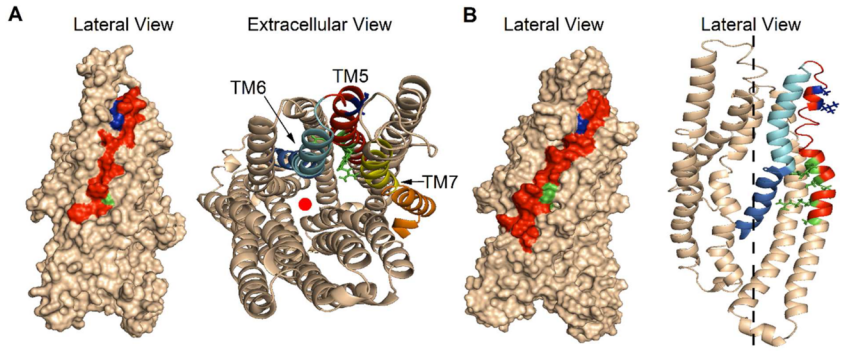

Figure 8. Lateral view and extracellular views of two outward-facing structural models of CFTR's TMDs, which represent the presumed open-channel conformation. The models were built on the basis of the crystal structure of a bacterial ABC transporter Sav1866. (A) Lateral view (left) with a surface representation and its extracellular view (right) with a ribbon representation of the modeled structure of Mornon et al.[19] The NBD1-RD (residues 370−850) and NBD2-C terminal (residues 1156−1480) are not shown here. Two TMDs of CFTR were colored wheat. Of note, the lateral view shows that the major portion of red-colored TM5 is located at the periphery of the CFTR protein and hence away from the centrally located pore. Positive hits for intracellular $MTSES^-$ are colored green, and two extracellular positive hits, L323 and A326, are colored blue. It is shown in the extracellular view that, while L323 and A326 are away from the pore axis (red solid circle), four of six of the intracellular positive hits (green) are pore-lining residues with their side chains exposed to the permeation pathway. F310 is buried in other TMs, and N306 is pointing to the lipid phase. Positions external to F312 are hidden behind the outer halves of TM6 (cyan) and TM7 (yellow). The cytoplasmic halves of TM6 (marine) and TM7 (orange) bent away from TM5 so that positions starting from F311 on TM5 are exposed to the pore. (B) Lateral view (left) of two TMDs of one outward-facing, "channel-like" CFTR homology model and its lateral view (right) of TMD1 with a ribbon representation developed by Dalton et al.[17] TMD2 has been omitted to better view the relative positions of TM5 and other TMs. The dashed line represents the pore axis. Color codes for all residues are the same as in panel A. The observations from both views are similar to those in panel A despite a significant difference in the arrangement of TMs in these two structures.

TM5 they tested turn out negative is consistent with our study. However, on the basis of our previous SCAM studies of TM1,[21] we have noted that some revisions of the amino acid assignment for CFTR's TM are necessary. In addition, the helical bundles that form the aqueous pore (or substrate translocation pathway) can easily extend beyond the traditionally defined membrane boundaries.[15,56−58] We thus expanded our cysteine scanning to include not only the whole putative TM5 defined by the original topological model[2] but also positions in the originally defined "intracellular loop". Our data suggest that this extended segment may not be a disordered loop but instead may assume a secondary structure and line the internal vestibule of CFTR's pore (also see below).

Among the six residues identified as pore-lining residues in TM5, the positively charged R303 is perhaps the most interesting one and relatively well studied. It was shown that the substitution of this arginine with glutamic acid results in strong outward rectification while wild-type CFTR shows a linear $I-V$ relationship under a symmetrical chloride condition.[35] Interestingly, the degree of rectification and the change in single-channel conductance depend on the charge status at position 303, consistent with the idea that the side chain of this residue exerts a pure electrostatic effect on the permeation of chloride through the pore. The same report also shows that a cysteine introduced at position 303 could be modified by either negatively charged $MTSES^-$ or positively charged $MTSET^+$. Indeed, some of these results are confirmed by the study presented here in a Cysless background (Figures 1, 3, and 7). Further support for the role of R303 in attracting anions comes from experiments using anionic CFTR pore blockers such as suramin, arachidonic acid, and tetranitroplatinate ($Pt[NO_2]_4^{2-}$). It was shown that blockade of CFTR by these reagents was significantly reduced by substitutions of R303 with glutamine or glutamic acid.[36,50,55] Thus, the importance of the positive charge at position 303 in the internal vestibule of CFTR's pore is beyond question. Here, we demonstrate that the R303C mutation in TM5 reduces glibenclamide block and modification by $MTSET^+$ almost completely restores the inhibition of glibenclamide (Figure 7). Taking all the experimental data together, we conclude that R303, as proposed previously,[32,35,36,50,55] plays an important role in the pore by attracting anions through a simple electrostatic effect. Then, the observation that this electrostatic role of R303 can be assumed by a positive charge introduced external to position 303 (Figure 7) constitutes another piece of evidence supporting the idea that TM5 lines part of the CFTR pore. Furthermore, the observation that bearing two positive charges at positions 303 and 306 yields an even higher single-channel current amplitude (Figure 7B,C) supports the idea that this part of the internal vestibule should be very spacious to prevent the creation of a strong anion binding trap.

Although the high-resolution structure of the whole CFTR protein has yet to be resolved, several homology models[16−20,59,60] have been built on the basis of the crystal structures of ABC exporters.[11,13] We next decided to look into these modeled structures with the hope of gaining some structural insights into our experimental results with TM5. Interestingly, in the latest outward-facing homology model reported by Norimatsu et al.,[16] the cytoplasmic boundary of TM5 is extended from S308 to A300, which coincides with the cytoplasmic edge in our SCAM study (i.e., A299). However, none of the pore-lining residues identified in this work are exposed to the anion permeation pathway according to this modeled structure. On the other hand, in another outward-facing homology model meant to simulate CFTR's open state[11,19] (Figure 8A), we found four of six positive positions are exposed to the channel pore, the exceptions being F310, which is buried in the protein, and N306, which faces the lipid bilayer. What is perhaps most intriguing to us is that in this modeled structure, the outer portion of TM5 (F312−K329) is concealed from the pore by resting behind the outer halves of TM6 and TM7 and the lipid bilayer. Of note, an early report by

DOI: 10.1021/acs.biochem.5b00427
Biochemistry 2015, 54, 3839−3850

Sheppard et al. that mutations at position 324 were without effect on the magnitude of the cAMP-stimulated CFTR current and the anion selectivity of CFTR is consistent with this picture.[61] Also strikingly, the cytoplasmic end (F312) of this buried segment in TM5 is identical to the internal accessibility limit identified in this study (Figure 1). A similar consistency between our data and computational predictions is also seen with another channel-like model published more recently[17] (Figure 8B).

While the modeled structures discussed above provide some satisfactory explanations for our data, we were somewhat perplexed by the concealment of N306 and F310 from the pore in these models. As the homology models so far examined all represent "open-channel conformations" of CFTR, it remains possible that these two positions may be exposed to the pore in the "closed" state. In the only homology model for CFTR's "closed-channel conformation" based on the bacterial ABC lipid flippase, MsbA,[13,18] we found that all six positive hits identified in our study are well-exposed in the aqueous pore and that the same outer segment of TM5 starting at F312 is obstructed by other TMs from the pore (Figure 9). Despite this surprisingly satisfying match between the modeled structures and our experimental data, we were not able to explain our SCAM results with L323C and A326C, two constructs responding to external $MTSES^-$ (Figure 2), as these two positions are part of the outer segment that is protruding to other TMs or membrane lipids. These structural models also fail to provide answers to explain two puzzling results. First, none of the 21 positions tested in TM7 are positive. Second, while F311C reacts to internal $MTSES^-$, $[Au(CN)_2]^-$ has little effect (Figure 3). Despite these caveats, these modeled structures of CFTR do support a role of TM5 in CFTR's pore construction, and our studies serve as a reminder that computational and experimental approaches could be fruitfully complementary in our pursuit of a better understanding of the CFTR channel.

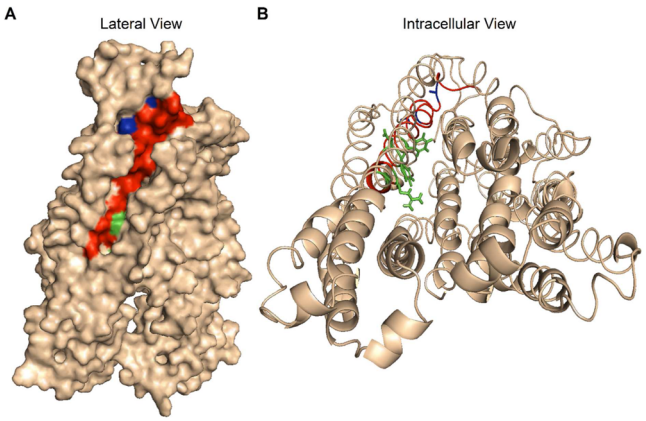

Figure 9. Lateral and cytoplasmic views of an inward-facing structural model representing the presumed closed conformation of CFTR. This model in ref 18 was based on the crystal structure of a bacterial ABC lipid flippase, MsbA. Color codes are the same as in Figure 8. (A) A lateral view with a surface representation shows that the majority of TM5 (red), including two extracellular positive hits, L323 and A326 (blue), is located at the periphery of the CFTR protein. (B) An intracellular view shows that all six positive hits with intracellular $MTSES^-$ are located on one face of TM5 where the side chains are exposed to the aqueous environment of the inner vestibule, whereas positions external to F312 (red and blue) are hidden behind other TMs.

■ ASSOCIATED CONTENT

Supporting Information

SCAM results on TM7, $MTSES^-$ modification on locked open N306C-CFTR, and a comparison of modification ratios on TM5 between macroscopic trace and single-channel current amplitude by $MTSES^-$ modification. The Supporting Information is available free of charge on the ACS Publications website at DOI: 10.1021/acs.biochem.5b00427.

■ AUTHOR INFORMATION

Corresponding Author

*Address: 222C DCRC Research Park, Columbia, MO 65211. E-mail: hwangt@health.missouri.edu. Phone: (573) 882-2181.

Author Contributions

J.Z. and T.-C.H. conceived and designed the experiments. J.Z. collected and analyzed the data. J.Z. and T.-C.H. interpreted the data. J.Z. and T.-C.H. drafted the article or revised it critically for important intellectual content. Both authors contributed equally to this work.

Funding

This work is supported by Grant R01DK55835 from the National Institutes of Health and a grant (Hwang13P0) from the Cystic Fibrosis Foundation (to T.-C.H.).

Notes

The authors declare no competing financial interest.

■ ACKNOWLEDGMENTS

We thank Cindy Chu and Shenghui Hu for their technical assistance. All experiments were performed in the Dalton Cardiovascular Research Center.

■ ABBREVIATIONS

ABC, ATP binding cassette; CFTR, cystic fibrosis transmembrane conductance regulator; NBD, nucleotide binding domain; TMD, transmembrane domain; TM, transmembrane segment; SCAM, substituted cysteine accessibility methodology; RD, regulatory domain; MTS, methanethiosulfonate; $MTSES^-$, 2-sulfonatoethyl MTS; $MTSET^+$, 2-trimethylaminoethyl MTS; $MTSEA^+$, 2-aminoethyl MTS hydrochloride; DTT, dithiothreitol; WT, wild type; $Pt[NO_2]_4^{2-}$, tetranitroplatinate; PP_i, pyrophosphate; Glib, glibenclamide.

■ REFERENCES

(1) Dean, M., and Annilo, T. (2005) Evolution of the ATP-binding cassette (ABC) transporter superfamily in vertebrates. *Annu. Rev. Genomics Hum. Genet. 6*, 123−142.

(2) Riordan, J. R., Rommens, J. M., Kerem, B., Alon, N., Rozmahel, R., Grzelczak, Z., Zielenski, J., Lok, S., Plavsic, N., Chou, J. L., et al. (1989) Identification of the cystic fibrosis gene: Cloning and characterization of complementary DNA. *Science 245*, 1066−1073.

(3) Bear, C. E., Li, C. H., Kartner, N., Bridges, R. J., Jensen, T. J., Ramjeesingh, M., and Riordan, J. R. (1992) Purification and functional reconstitution of the cystic fibrosis transmembrane conductance regulator (CFTR). *Cell 68*, 809−818.

(4) Moskowitz, S. M., Chmiel, J. F., Sternen, D. L., Cheng, E., Gibson, R. L., Marshall, S. G., and Cutting, G. R. (2008) Clinical practice and genetic counseling for cystic fibrosis and CFTR-related disorders. *Genet. Med. 10*, 851−868.

DOI: 10.1021/acs.biochem.5b00427
Biochemistry 2015, 54, 3839−3850

(5) Hwang, T. C., and Kirk, K. L. (2013) The CFTR ion channel: Gating, regulation, and anion permeation. *Cold Spring Harbor Perspect. Med. 3*, a009498.
(6) Gadsby, D. C., Vergani, P., and Csanády, L. (2006) The ABC protein turned chloride channel whose failure causes cystic fibrosis. *Nature 440*, 477−483.
(7) Hwang, T. C., and Sheppard, D. N. (2009) Gating of the CFTR Cl^- channel by ATP-driven nucleotide-binding domain dimerisation. *J. Physiol. 587*, 2151−2161.
(8) Chen, T. Y., and Hwang, T. C. (2008) CLC-0 and CFTR: Chloride Channels Evolved From Transporters. *Physiol. Rev. 88*, 351−387.
(9) Csanady, L., and Torocsik, B. (2014) Catalyst-like modulation of transition states for CFTR channel opening and closing: New stimulation strategy exploits nonequilibrium gating. *J. Gen. Physiol. 143*, 269−287.
(10) Jih, K. Y., and Hwang, T. C. (2012) Nonequilibrium gating of CFTR on an equilibrium theme. *Physiology 27*, 351−361.
(11) Dawson, R. J. P., and Locher, K. P. (2006) Structure of a bacterial multidrug ABC transporter. *Nature 443*, 180−185.
(12) Dawson, R. J. P., and Locher, K. P. (2007) Structure of the multidrug ABC transporter Sav1866 from *Staphylococcus aureus* in complex with AMP-PNP. *FEBS Lett. 581*, 935−938.
(13) Ward, A., Reyes, C. L., Yu, J., Roth, C. B., and Chang, G. (2007) Flexibility in the ABC transporter MsbA: Alternating access with a twist. *Proc. Natl. Acad. Sci. U.S.A. 104*, 19005−19010.
(14) Aller, S. G., Yu, J., Ward, A., Weng, Y., Chittaboina, S., Zhuo, R., Harrell, P. M., Trinh, Y. T., Zhang, Q., Urbatsch, I. L., and Chang, G. (2009) Structure of P-Glycoprotein Reveals a Molecular Basis for Poly-Specific Drug Binding. *Science 323*, 1718−1722.
(15) Hohl, M., Briand, C., Grutter, M. G., and Seeger, M. A. (2012) Crystal structure of a heterodimeric ABC transporter in its inward-facing conformation. *Nat. Struct. Mol. Biol. 19*, 395−402.
(16) Norimatsu, Y., Ivetac, A., Alexander, C., Kirkham, J., O'Donnell, N., Dawson, D. C., and Sansom, M. S. (2012) Cystic fibrosis transmembrane conductance regulator: A molecular model defines the architecture of the anion conduction path and locates a "bottleneck" in the pore. *Biochemistry 51*, 2199−2212.
(17) Dalton, J., Kalid, O., Schushan, M., Ben-Tal, N., and Villa-Freixa, J. (2012) New model of cystic fibrosis transmembrane conductance regulator proposes active channel-like conformation. *J. Chem. Inf. Model. 52*, 1842−1853.
(18) Mornon, J. P., Lehn, P., and Callebaut, I. (2009) Molecular models of the open and closed states of the whole human CFTR protein. *Cell. Mol. Life Sci. 66*, 3469−3486.
(19) Mornon, J. P., Lehn, P., and Callebaut, I. (2008) Atomic model of human cystic fibrosis transmembrane conductance regulator: Membrane-spanning domains and coupling interfaces. *Cell. Mol. Life Sci. 65*, 2594−2612.
(20) Mornon, J. P., Hoffmann, B., Jonic, S., Lehn, P., and Callebaut, I. (2015) Full-open and closed CFTR channels, with lateral tunnels from the cytoplasm and an alternative position of the F508 region, as revealed by molecular dynamics. *Cell. Mol. Life Sci. 72*, 1377−1403.
(21) Gao, X., Bai, Y., and Hwang, T. C. (2013) Cysteine scanning of CFTR's first transmembrane segment reveals its plausible roles in gating and permeation. *Biophys. J. 104*, 786−797.
(22) Akabas, M. H. (1998) Channel-lining residues in the M3 membrane-spanning segment of the cystic fibrosis transmembrane conductance regulator. *Biochemistry 37*, 12233−12240.
(23) Bai, Y., Li, M., and Hwang, T. C. (2010) Dual roles of the sixth transmembrane segment of the CFTR chloride channel in gating and permeation. *J. Gen. Physiol. 136*, 293−309.
(24) El Hiani, Y., and Linsdell, P. (2010) Changes in accessibility of cytoplasmic substances to the pore associated with activation of the cystic fibrosis transmembrane conductance regulator chloride channel. *J. Biol. Chem. 285*, 32126−32140.
(25) Jordan, I. K., Kota, K. C., Cui, G., Thompson, C. H., and McCarty, N. A. (2008) Evolutionary and functional divergence between the cystic fibrosis transmembrane conductance regulator and related ATP-binding cassette transporters. *Proc. Natl. Acad. Sci. U.S.A. 105*, 18865−18870.
(26) Fatehi, M., and Linsdell, P. (2009) Novel Residues Lining the CFTR Chloride Channel Pore Identified by Functional Modification of Introduced Cysteines. *J. Membr. Biol. 228*, 151−164.
(27) Qian, F., El Hiani, Y., and Linsdell, P. (2011) Functional arrangement of the 12th transmembrane region in the CFTR chloride channel pore based on functional investigation of a cysteine-less CFTR variant. *Pfluegers Arch. 462*, 559−571.
(28) Bai, Y., Li, M., and Hwang, T. C. (2011) Structural basis for the channel function of a degraded ABC transporter, CFTR (ABCC7). *J. Gen. Physiol. 138*, 495−507.
(29) Wang, W., and Linsdell, P. (2012) Alternating Access to the Transmembrane Domain of the ATP-binding Cassette Protein Cystic Fibrosis Transmembrane Conductance Regulator (ABCC7). *J. Biol. Chem. 287*, 10156−10165.
(30) Wang, W., El Hiani, Y., Rubaiy, H. N., and Linsdell, P. (2014) Relative contribution of different transmembrane segments to the CFTR chloride channel pore. *Pfluegers Arch. 466*, 477−490.
(31) Ge, N., Muise, C. N., Gong, X., and Linsdell, P. (2004) Direct comparison of the functional roles played by different transmembrane regions in the cystic fibrosis transmembrane conductance regulator chloride channel pore. *J. Biol. Chem. 279*, 55283−55289.
(32) Linsdell, P. (2005) Location of a common inhibitor binding site in the cytoplasmic vestibule of the cystic fibrosis transmembrane conductance regulator chloride channel pore. *J. Biol. Chem. 280*, 8945−8950.
(33) Wang, W., and Linsdell, P. (2012) Conformational change opening the CFTR chloride channel pore coupled to ATP-dependent gating. *Biochim. Biophys. Acta 1818*, 851−860.
(34) Zhou, J. J., Li, M. S., Qi, J., and Linsdell, P. (2010) Regulation of conductance by the number of fixed positive charges in the intracellular vestibule of the CFTR chloride channel pore. *J. Gen. Physiol. 135*, 229−245.
(35) Aubin, C. N., and Linsdell, P. (2006) Positive charges at the intracellular mouth of the pore regulate anion conduction in the CFTR chloride channel. *J. Gen. Physiol. 128*, 535−545.
(36) Zhou, J. J., Fatehi, M., and Linsdell, P. (2007) Direct and indirect effects of mutations at the outer mouth of the cystic fibrosis transmembrane conductance regulator chloride channel pore. *J. Membr. Biol. 216*, 129−142.
(37) Cui, G., Zhang, Z. R., O'Brien, A. R., Song, B., and McCarty, N. A. (2008) Mutations at arginine 352 alter the pore architecture of CFTR. *J. Membr. Biol. 222*, 91−106.
(38) Guinamard, R., and Akabas, M. H. (1999) Arg352 is a major determinant of charge selectivity in the cystic fibrosis transmembrane conductance regulator chloride channel. *Biochemistry 38*, 5528−5537.
(39) Cheung, M., and Akabas, M. H. (1997) Locating the anion-selectivity filter of the cystic fibrosis transmembrane conductance regulator (CFTR) chloride channel. *J. Gen. Physiol. 109*, 289−299.
(40) Liu, X., Alexander, C., Serrano, J., Borg, E., and Dawson, D. C. (2006) Variable Reactivity of an Engineered Cysteine at Position 338 in Cystic Fibrosis Transmembrane Conductance Regulator Reflects Different Chemical States of the Thiol. *J. Biol. Chem. 281*, 8275−8285.
(41) Li, Y., Yu, W.-P., Lin, C.-W., and Chen, T.-Y. (2005) Oxidation and Reduction Control of the Inactivation Gating of Torpedo ClC-0 Chloride Channels. *Biophys. J. 88*, 3936−3945.
(42) McCarty, N. A. (2000) Permeation through the CFTR chloride channel. *J. Exp. Biol. 203*, 1947−1962.
(43) Melis, N., Tauc, M., Cougnon, M., Bendahhou, S., Giuliano, S., Rubera, I., and Duranton, C. (2014) Revisiting CFTR inhibition: A comparative study of CFTRinh-172 and GlyH-101 inhibitors. *Br. J. Pharmacol. 171*, 3716−3727.
(44) Norimatsu, Y., Ivetac, A., Alexander, C., O'Donnell, N., Frye, L., Sansom, M. S., and Dawson, D. C. (2012) Locating a plausible binding site for an open-channel blocker, GlyH-101, in the pore of the cystic fibrosis transmembrane conductance regulator. *Mol. Pharmacol. 82*, 1042−1055.

DOI: 10.1021/acs.biochem.5b00427
Biochemistry 2015, 54, 3839−3850

(45) Serrano, J. R., Liu, X., Borg, E. R., Alexander, C. S., Shaw, C. F., and Dawson, D. C. (2006) CFTR: Ligand Exchange between a Permeant Anion ($[Au(CN)_2]^-$) and an Engineered Cysteine (T338C) Blocks the Pore. *Biophys. J. 91*, 1737−1748.
(46) Zhou, Z., Hu, S., and Hwang, T. C. (2002) Probing an open CFTR pore with organic anion blockers. *J. Gen. Physiol. 120*, 647−662.
(47) Sheppard, D. N., and Robinson, K. A. (1997) Mechanism of glibenclamide inhibition of cystic fibrosis transmembrane conductance regulator Cl^- channels expressed in a murine cell line. *J. Physiol. 503* (Part 2), 333−346.
(48) Schultz, B. D., DeRoos, A. D., Venglarik, C. J., Singh, A. K., Frizzell, R. A., and Bridges, R. J. (1996) Glibenclamide blockade of CFTR chloride channels. *Am. J. Physiol. 271*, L192−L200.
(49) Zhang, Z. R., Cui, G., Zeltwanger, S., and McCarty, N. A. (2004) Time-dependent interactions of glibenclamide with CFTR: Kinetically complex block of macroscopic currents. *J. Membr. Biol. 201*, 139−155.
(50) St Aubin, C. N., Zhou, J. J., and Linsdell, P. (2007) Identification of a second blocker binding site at the cytoplasmic mouth of the cystic fibrosis transmembrane conductance regulator chloride channel pore. *Mol. Pharmacol. 71*, 1360−1368.
(51) Gupta, J., and Linsdell, P. (2002) Point mutations in the pore region directly or indirectly affect glibenclamide block of the CFTR chloride channel. *Pfluegers Arch. 443*, 739−747.
(52) Melin, P., Hosy, E., Vivaudou, M., and Becq, F. (2007) CFTR inhibition by glibenclamide requires a positive charge in cytoplasmic loop three. *Biochim. Biophys. Acta 1768*, 2438−2446.
(53) Cui, G., Song, B., Turki, H. W., and McCarty, N. A. (2012) Differential contribution of TM6 and TM12 to the pore of CFTR identified by three sulfonylurea-based blockers. *Pfluegers Arch. 463*, 405−418.
(54) Mansoura, M. K., Smith, S. S., Choi, A. D., Richards, N. W., Strong, T. V., Drumm, M. L., Collins, F. S., and Dawson, D. C. (1998) Cystic fibrosis transmembrane conductance regulator (CFTR) anion binding as a probe of the pore. *Biophys. J. 74*, 1320−1332.
(55) Zhou, J. J., and Linsdell, P. (2007) Molecular mechanism of arachidonic acid inhibition of the CFTR chloride channel. *Eur. J. Pharmacol. 563*, 88−91.
(56) Kodan, A., Yamaguchi, T., Nakatsu, T., Sakiyama, K., Hipolito, C. J., Fujioka, A., Hirokane, R., Ikeguchi, K., Watanabe, B., Hiratake, J., Kimura, Y., Suga, H., Ueda, K., and Kato, H. (2014) Structural basis for gating mechanisms of a eukaryotic P-glycoprotein homolog. *Proc. Natl. Acad. Sci. U.S.A. 111*, 4049−4054.
(57) Hollenstein, K., Dawson, R. J. P., and Locher, K. P. (2007) Structure and mechanism of ABC transporter proteins. *Curr. Opin. Struct. Biol. 17*, 412−418.
(58) Opella, S. J., Marassi, F. M., Gesell, J. J., Valente, A. P., Kim, Y., Oblatt-Montal, M., and Montal, M. (1999) Structures of the M2 channel-lining segments from nicotinic acetylcholine and NMDA receptors by NMR spectroscopy. *Nat. Struct. Biol. 6*, 374−379.
(59) Alexander, C., Ivetac, A., Liu, X., Norimatsu, Y., Serrano, J. R., Landstrom, A., Sansom, M., and Dawson, D. C. (2009) Cystic Fibrosis Transmembrane Conductance Regulator: Using Differential Reactivity toward Channel-Permeant and Channel-Impermeant Thiol-Reactive Probes To Test a Molecular Model for the Pore. *Biochemistry 48*, 10078−10088.
(60) Serohijos, A. W., Thibodeau, P. H., and Dokholyan, N. V. (2011) Molecular modeling tools and approaches for CFTR and cystic fibrosis. *Methods Mol. Biol. 741*, 347−363.
(61) Sheppard, D. N., Travis, S. M., Ishihara, H., and Welsh, M. J. (1996) Contribution of proline residues in the membrane-spanning domains of cystic fibrosis transmembrane conductance regulator to chloride channel function. *J. Biol. Chem. 271*, 14995−15001.

DOI: 10.1021/acs.biochem.5b00427
Biochemistry 2015, 54, 3839−3850